Communication

Not peer-reviewed version

Effect of Film Thickness on Microstructural and Magnetic Properties of Lithium Ferrite Films Prepared on $SrTiO_3$ (001) Substrates

Kun Liu , Ruyi Zhang , Lu Lu * , Jiankang Li , Songyou Zhang

Posted Date: 17 November 2023

doi: 10.20944/preprints202309.1631.v2

Keywords: Lithium ferrite; Film thickness; Defects; Magnetic properties; Electron microscopy

Article

Effect of Film Thickness on Microstructural and Magnetic Properties of Lithium Ferrite Films Prepared on $SrTiO_3$ (001) Substrates

Kun Liu [1], Ruyi Zhang [2], Lu Lu [3,*], Jiankang Li [1] and Songyou Zhang [1]

[1] School of Electronics and Information Engineering, Suzhou Vocational University, Su Zhou 215104, China
[2] Ningbo Institute of Materials Technology and Engineering, Chinese Academy of Sciences, Ningbo 315201, China
[3] Ji Hua Laboratory, Foshan 528200, China
* Correspondence: lulu@jihualab.ac.cn

Abstract: Epitaxial lithium ferrite ($LiFe_5O_8$) films with different thicknesses have been successfully fabricated on $SrTiO_3$ (001) substrates by magnetron sputtering deposition technique. The microstructural and magnetic properties are characterized by advanced transmission electron microscope and magnetic measurement device. It was found that the formation of structural defects can be influenced by the thickness of the film. Apart from the misfit dislocations, the orientation domains form in thinner film and twin boundaries appear in thicker film, respectively, contributing to the misfit strain relaxation in the heterosystem. The magnetic measurement shows that the thinner films have enhanced magnetization and a relatively lower coercive field compared with the thicker films containing the antiferromagnetic twin boundaries. Our results provide a way for tuning the microstructure and magnetic properties of lithium ferrite films by changing the film thickness.

Keywords: lithium ferrite; film thickness; defects; magnetic properties; electron microscopy

1. Introduction

Lithium ferrite ($LiFe_5O_8$) has drawn widespread attention of research because of its remarkable physical properties, such as high saturation magnetization, high Curie temperature, large electric resistivity, low loss at high frequencies, and good chemical and thermal stability [1,2], which make it have potential application in components of microwave device and spintronics [3,4]. $LiFe_5O_8$ has the inverse spinel structure, where the tetrahedral sites are occupied by Fe^{3+}, and the octahedral sites are shared by Li^+ and the rest Fe^{3+} in a ratio of 1:3 (denoted as $Fe[Li_{0.5}Fe_{1.5}]O_4$). The antiparallel aligned magnetic spin between the Fe^{3+} distributing at tetrahedral sites and octahedral sites leads to a high magnetic moment of 2.5 μB per formula unit [1,5]. Compared to the bulk material, spinel thin films exhibit microstructural variations such as the presence of planar defects, which can alter the electrical and magnetic structures of the films [6,7]. Thus, research efforts concentrating on the growth, structure, property, and applications of the spinel thin films have proliferated over the last decades [8–10].

Generally, during the film deposition process, many degrees of freedom can be used to modify the structural and physical properties of the film [11–13]. Among them, changing the film thickness is a common method to manipulate the strain state of the film [14,15]. Particularly, tuning strain states not only cause the formation of oriented domains [16,17], but also lead to the different density of antiphase boundaries in spinel films [18,19], which influence the magnetic properties of the films consequently [20]. Moreover, enhanced magnetic moments are present in ultrathin films (e.g., $NiFe_2O_4$ and $CoFe_2O_4$) prepared on spinel-type $MgAl_2O_4$ substrates [21–23]. In contrast, there are limited investigations on the microstructural characteristic and magnetic behavior of $LiFe_5O_8$ films

 doi:10.20944/preprints202309.1631.v2

with different thickness prepared on perovskite-type substrates that are widely used as substrates for growing functional films in device application.

In the present work, the microstructural and magnetic properties of $LiFe_5O_8$ films with two different thicknesses prepared on $SrTiO_3$ substrates have been investigated by aberration-corrected (scanning) transmission electron microscopy ((S)TEM) and superconducting quantum interference device (SQUID). The twin boundaries (TBs), orientation domains, and interface dislocation in the films have been determined by high-angle annular dark-field (HAADF) imaging. The magnetic properties of the films have been characterized by magnetization measurement in a SQUID magnetometer, and the effect of film thickness and structure defects on the magnetic properties of the $LiFe_5O_8$ films has been discussed. This investigation provides a way of changing the thickness to manipulate the microstructure and the magnetic properties of $LiFe_5O_8$ films, making them adapt to diverse technological applications, e.g., electrode for rechargeable lithium-ion batteries, various components in microwave devices, and magnetic insulators for spin filtering in spintronics [24–26].

2. Materials and Methods

$LiFe_5O_8$ ceramic target was prepared by a standard solid-state reaction method with the initial reactants Fe_2O_3 and $LiCO_3$ (ratio 5:2). The $LiFe_5O_8$ films with different thicknesses were fabricated on single-crystalline $SrTiO_3$ (001) substrates by a high-pressure sputtering system at the substrate temperature of 800 °C. The working pressure was 0.5 mbar with the mixed ambient of Ar and O_2 at the ratio of 1:1.

(S)TEM specimens were prepared by focused ion beam (FIB) lift-out technique using an FEI Helios600i FIB/SEM system. FIB lamellae were cut along the <110> orientations of the $SrTiO_3$ substrate. TEM and HAADF-STEM experiments were performed on a JEOL-ARM200F with a probe aberration corrector, operated at 200 kV. In STEM mode, a probe size of 0.1 nm at semi-convergence angle of 22 mrad was used for HAADF-STEM imaging. The HAADF detectors covered angular ranges of 90-176 mrad. The magnetic hysteresis (M-H) loops were measured by a SQUID (Quantum Design) with magnetic field applied along STO [100] and [001] directions, respectively. The quartz paddle and brass half-tube were used as sample holders for M-H loops along in-plane (STO [100] direction) and out-of-plane (STO [001] direction), respectively.

3. Results and discussions

Figure 1a and 1b are the low-magnification bright-field (BF) TEM images of $LiFe_5O_8$ thin film on $SrTiO_3$(001) substrates with a thickness of 7.5 nm and 30 nm, respectively. The film-substrate interfaces are marked by horizontal arrows. The contrast variation within the film can be discerned in both films. In Figure 1b, the oblique contrast lines shown by blue arrows are apparent. Figure 1c and 1d display the corresponding selected area electron diffraction (SAED) pattern of the heterostructure in Figure 1a and 1b, respectively, recorded along the $[1\bar{1}0]$ zone axis of $SrTiO_3$. In Figure 1c, apart from the diffraction spots of the $SrTiO_3$ substrate, two sets of diffraction spots from the $LiFe_5O_8$ film can be distinguished, resulting in two film-substrate orientation relationships (ORs) as $[1\bar{1}0](001)_{film}//[1\bar{1}0](001)_{substrate}$ (cube-on-cube) and $[1\bar{1}0](111)_{film}//[1\bar{1}0](001)_{substrate}$. Considering the four-fold symmetry of the $SrTiO_3$(001) substrate surface, there exists an equivalent OR having a 90° in-plane orientation relation to the latter OR. In Figure 1d, the $LiFe_5O_8$ film adopts the cube-on-cube OR with the substrate. Instead of forming crystalline orientation domains in the 7.5-nm-thick film, there present some {111} TBs in the 30-nm-thick film. Taking the lattice parameter of $SrTiO_3$ substrate (0.3905 nm) as the calibration standard [27], the in-plane and out-of-plane lattice parameter of the 7.5-nm-thick film is calculated to be 0.8319 nm and 0.8353 nm, respectively. Similarly, in-plane and out-of-plane lattice parameter of the 30-nm-thick film is calculated to be 0.8301 nm and 0.8359 nm, respectively. All the parameters are close to that of the bulk material, indicating that the considerable mismatch strain of both films is relaxed, leaving tender compressive strain in the film [10].

Preprints (www.preprints.org) | NOT PEER-REVIEWED | Posted: 17 November 2023 doi:10.20944/preprints202309.1631.v2

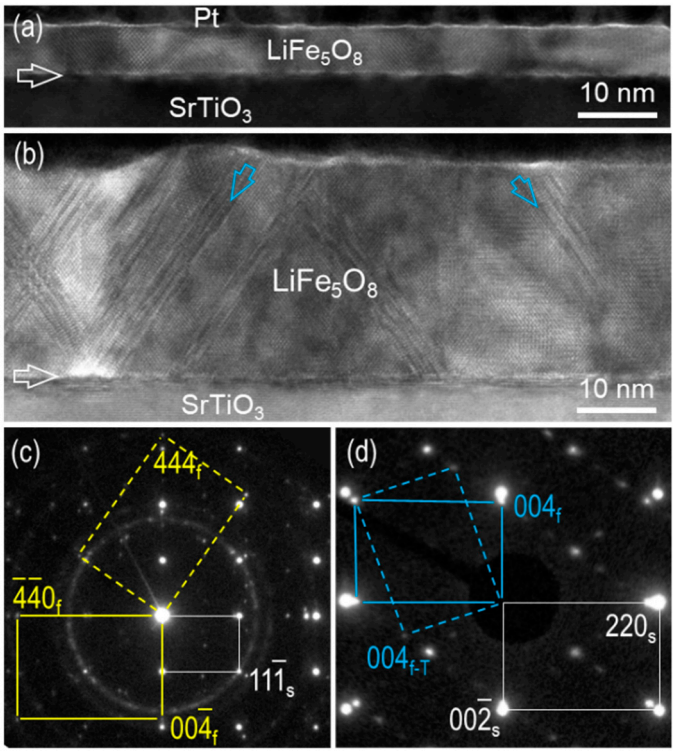

Figure 1. (a, b) Low-magnification BF-TEM images and (c, d) the corresponding SAED patterns of 7.5-nm-thick and 30-nm-thick $LiFe_5O_8$ film prepared on $SrTiO_3$ (001) substrate, recorded along the $[1\bar{1}0]$ $SrTiO_3$ zone axes. The film-substrate interface is indicated by horizontal arrows. The twin boundary is denoted by oblique blue arrows.

In order to further investigate the microstructure and strain relaxation behaviors, high-resolution HAADF-STEM experiments have been performed. Figure 2a–2c are the atomic-resolution HAADF-STEM images showing the interfaces of the 7.5-nm-thick film, viewed along $[1\bar{1}0]$ zone axis of the $SrTiO_3$ substrate. Misfit dislocations form at the interface in both heterostructures. For the grain with the cube-on-cube OR (Figure 2a), the projected Burgers vector of misfit dislocations can be determined as $(a_f/4)[110]$ (a_f is the lattice parameter of $LiFe_5O_8$). For the $[1\bar{1}0](111)_{film}//[1\bar{1}0](001)_{substrate}$ OR, the misfit dislocations occur at the interfaces, as shown in Figure 2b and 2c. The projected Burgers vectors are determined to be $(a_f/8)[11\ \bar{2}\ ]$ and $(a_f/4)[1\ \bar{1}\ 0]$, respectively. In contrast, for the heterostructure of the 30-nm-thick film on the $SrTiO_3$(001) substrate, only a number of {111} TBs appear within the $LiFe_5O_8$ film as demonstrated in Figure 2d. It should be noted that abnormal contrast has not been observed in any HAADF images, indicating there is no chemical segregation in the film.

Preprints (www.preprints.org) | NOT PEER-REVIEWED | Posted: 17 November 2023 doi:10.20944/preprints202309.1631.v2

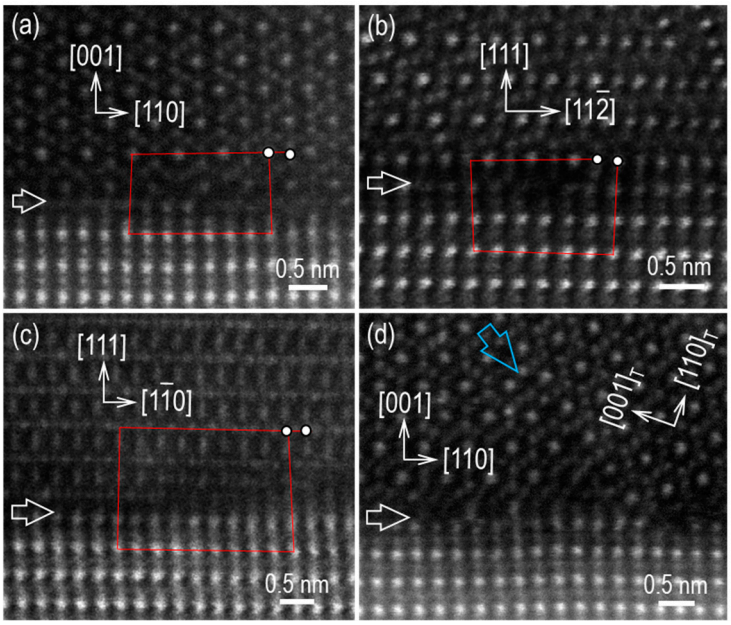

Figure 2. (a~d) High-resolution HAADF-STEM images of the heterostructures, viewed along the [1 $\bar{1}$0] $SrTiO_3$ zone axis, showing the formation of misfit dislocations and twin boundaries. The film-substrate interfaces are denoted by horizontal white arrows.

Additionally, for the heterostructure of the 7.5-nm-thick film prepared on $SrTiO_3$(001) substrate, the occurrence of two types of film-substrate ORs would form a columnar grain structure in the film. The coalescence of these grains inevitably leads to the formation of grain boundaries (GBs). Figure 3a–3c are the HAADF-STEM images containing such GBs. The boundaries appear curved through the film as traced by white dashed lines. It should be emphasized that there is no secondary phase or obvious element segregation at the boundaries.

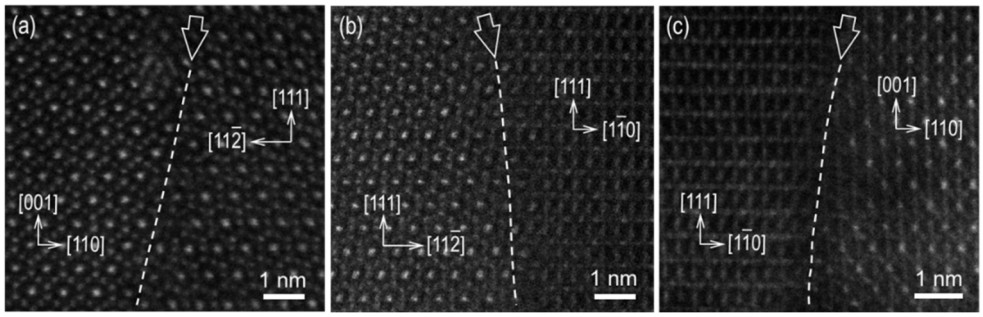

Figure 3. (a~c) HAADF-STEM images of grain boundaries in 7.5-nm-thick film. The boundaries are denoted by white dashed lines and oblique white arrows.

In the $LiFe_5O_8$/$SrTiO_3$ heterostructure, the lattice mismatch is calculated to be about +6.2% for cube-on-cube epitaxy, using the formula $[(a_f\text{-}2a_s)/2a_s]$*100%. For the $LiFe_5O_8$(111)/$SrTiO_3$(001) epitaxy, the lattice mismatch along $[110]_f$ direction is the same as that of the cube-on-cube epitaxy, whereas the film-substrate lattice mismatch along $[11\bar{2}]_f$ direction is much large. Based on the TEM results, different strain relaxation behaviors occur in the $LiFe_5O_8$ films through different defect configurations [28,29]. The appearance of oriented grains and misfit dislocations releases the compressive strain in the 7.5-nm-thick film on $SrTiO_3$ substrate. In contrast, the formation of a high density of twins within the film mainly contributes to the strain relaxation in the 30-nm-thick film.

The magnetic properties of the $LiFe_5O_8$ films have been characterized by the magnetic hysteresis loops using the SQUID system. The effect of pure $SrTiO_3$ substrate has been carefully eliminated. Figure 4a and 4b present the M-H hysteresis loops measured along in-plane and out-of-plane directions of 7.5-nm- and 30-nm-thick film separately. The in-plane saturation magnetization (Ms) of

Preprints (www.preprints.org) | NOT PEER-REVIEWED | Posted: 17 November 2023 doi:10.20944/preprints202309.1631.v2

the 7.5-nm-thick film is about 583 emu/cc and the out-of-plane Ms is 465 emu/cc (experimental error for the magnetization (± 1 emu/cc)). Both values are significantly higher than that of bulk $LiFe_5O_8$ (2.5 μB/formula unit ~ 320 emu/cc) [5]. The in-plane and the out-of-plane Ms of the 30-nm-thick film are about 204 emu/cc and 154 emu/cc, respectively. The 7.5-nm-thick film exhibits considerable high Ms compared with the values in literature (see Table I in Supplementary Material). The in-plane and out-of-plane coercive fields (Hc) of the 7.5-nm-thick film are about 50 Oe and 101 Oe, respectively, which are slightly smaller than that of the 30-nm-thick film (254 Oe and 140 Oe) (experimental error for experimental error for coercivity values (± 10 Oe)). Our measurement of the magnetic properties shows apparent thickness dependence of $LiFe_5O_8$ thin films prepared on $SrTiO_3$(001) substrates.

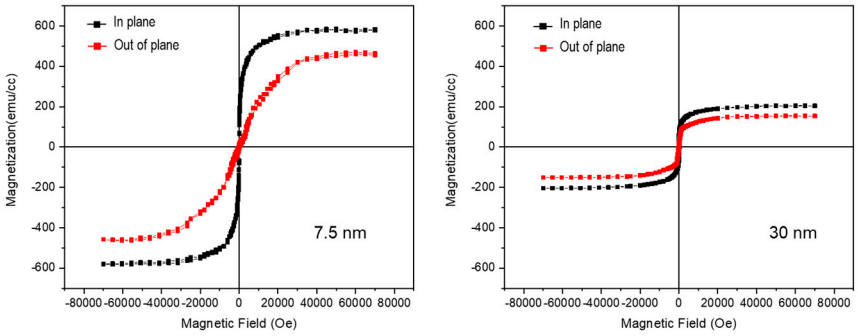

Figure 4. (a, b) In-plane and out-of-plane magnetic hysteresis loops of $LiFe_5O_8$ films with different thicknesses measured at room temperature (300 K).

The enhancement of the magnetization and the decrease of the coercive field has been reported in thinner spinel films, e.g., $NiFe_2O_4$ and $CoFe_2O_4$ [21–23] and $LiFe_5O_8$ on $MgAl_2O_4$ substrates [10]. The anomalous cation distribution among the tetrahedral and octahedral sites of the spinel structure has been invoked to account for this phenomenon [14,21]. In our $LiFe_5O_8$ thin films, no chemical modulation or second phase has been observed during TEM investigations, ruling out the anomalous Fe^{3+} distribution as the origin of the enhanced Ms. Thus, the most likely factor responsible for the thickness-dependent magnetic properties is the strain state and the microstructure of the film. It is considered that the enhanced Ms in the 7.5-nm-thick film is due to the distinct column grain structure and the possible oxygen vacancies at the GBs. The presence of oxygen vacancies is associated with the reduced ions Fe^{2+}, which can mitigate the antiparallel aligned spin of Fe^{3+} at tetrahedral sites and octahedral sites, resulting in enhancement of the net magnetic moment [1,30]. In contrast, the appearance of a high density of TBs with antiferromagnetic coupling [7] in the 30-nm-thick film will weaken the Ms of the film [31].

$LiFe_5O_8$ is a negative magnetostrictive material with saturation magnetostriction ~27.8 ppm [10]. The compressive strain favors the in-plane orientation of the magnetization [22,32]. Although strain relaxations occur in our $LiFe_5O_8$ films, the tetragonal lattice distortions appear in both films under compressive strain, resulting in anisotropic magnetization in the both films. The coercive fields (Hc) of 30 nm film are slightly higher than that of 7.5nm film. The occurrence of antiferromagnetic defects and effect of magnetic domain wall pinning induced by those defects are likely to make it difficult to turn over the magnetic domain during magnetization process, which leads to the larger coercive field in 30 nm film. Overall, varying thicknesses of the $LiFe_5O_8$ films on $SrTiO_3$(001) substrate can effectively modify the microstructural and magnetic properties of the film.

4. Conclusion

The epitaxial $LiFe_5O_8$ thin films with the thickness of 7.5 nm and 30 nm have been grown on $SrTiO_3$ (001) substrate. Microstructural investigations show that the $(111)_{film}//(001)_{substrate}$ and $(001)_{film}//(001)_{substrate}$ ORs appear in the 7.5-nm-thick film, and TBs occur in the 30-nm-thick film, respectively, which contributes to the lattice misfit strain. Importantly, the 7.5-nm-thick film displays

a larger saturation magnetization and a relatively lower coercive field in comparison with the 30-nm-thick film. Our results demonstrate that changing the film thickness could effectively tune the microstructure and magnetic properties in epitaxial $LiFe_5O_8$ thin film.

Author Contributions: Conceptualisation, K.L.; investigation, K.L, R.Z; writing—original draft preparation, K.L.; writing—review and editing, L.L., J.L, S.Z.; supervision, L.L. All authors have read and agreed to the published version of the manuscript.

Funding: This research was funded by the Guangdong Major Project of Basic and Applied Basic Research (No. 2021B0301030003), the Science and Technology Planning Project of Suzhou City (No. SZS2022015), the Natural Science Foundation of the Jiangsu Higher Education Institutions of China (Grant: 21KJB510022) and Cultivation project of Suzhou vocational University (SVU2021py02).

Institutional Review Board Statement: Not applicable.

Informed Consent Statement: Not applicable.

Data Availability Statement: Not applicable.

Acknowledgments: Thanks to Suzhou Key Laboratory of Smart Energy Technology, Jihua Laboratory for the support of experiments of characterization.

Conflicts of Interest: The authors declare no conflict of interest.

References

1. White, G.O.; Patton, C.E. Magnetic Properties of Lithium Ferrite Microwave Materials, J. Magn. Magn. Mater. **1978**, 9(4), 299-317.
2. Sugimoto, M. The Past, Present, and Future of Ferrites, J. Am. Ceram. Soc. **1999**, 82(2), 269-280.
3. Lüders, U.; Barthélémy, A.; Bibes, M.; Bouzehouane, K.; Fusil, S.; Jacquet, E.; Contour, J.-P.; Bobo, J.-F.; J.-F. Fontcuberta, J.-F.; Fert, A. $NiFe_2O_4$: A Versatile Spinel Material Brings New Opportunities for Spintronics, Adv. Mater. **2006**, 18(13), 1733-1736.
4. Suzuki, Y. Epitaxial Spinel Ferrite Thin Films, Annual Review of Materials Research **2001**, 31, 265-289.
5. Boyraz, C.; Mazumdar, D.; Iliev, M.; Marinova, V.; Ma, J.; Srinivasan, G.; Gupta, A. Structural and magnetic properties of lithium ferrite ($LiFe_5O_8$) thin films: Influence of substrate on the octahedral site order, Appl. Phys. Lett. **2011**, 98(1), 012507.
6. Wei, J. D.; Knittel, I.; Hartmann, U.; Zhou, Y.; Murphy, S.; Shvets, I. V. et al. Influence of the Antiphase Domain Distribution on the Magnetic Structure of Magnetite Thin Films, Appl. Phys. Lett. **2006**, 89(12), 122517.
7. Chen, C. L.; Li, H. P.; Seki, T.; Yin, D. Q.; Sanchez-Santolino, G.; Inoue, K et al. Direct Determination of Atomic Structure and Magnetic Coupling of Magnetite Twin Boundaries, ACS nano, **2008**, 12(3), 2662-2668.
8. Udhayakumar, S.; Kumar, G. J.; Kumar, E. S.; Navaneethan, M.; Kamala Bharathi, K. Electrical, Electronic and Magnetic Property Correlation Via Oxygen Vacancy Filling and Scaling-law Analysis in $LiFe_5O_8$ Thin Films Prepared by Pulsed Laser Deposition, J. Mater. Chem. C **2022**, 10(40), 15051-15060.
9. Liu, X.; Wu, M.; Qu, K.; Gao, P.; Mi, W. Atomic-Scale Mechanism of Grain Boundary Effects on the Magnetic and Transport Properties of Fe_3O_4 Bicrystal Films, ACS Appl. Mater. and Inter. **2021**, 13(5), 6889-6896.
10. Zhang, R.; Liu, M.; Lu, L.; Mi, S.B.; Wang, H. Strain-tunable magnetic properties of epitaxial lithium ferrite thin film on $MgAl_2O_4$ substrates, J. Mater. Chem. C **2015**, 3(21), 5598-5602.
11. Hu, G.; Choi, J. H.; Eom, C. B.; Harris, V. G.; Suzuki, Y. Structural Tuning of the Magnetic Behavior in Spinel-Structure Ferrite Thin Films, Phys. Rev. B **2000**, 62(2), R779-R782.
12. Uusi-Esko, K.; Rautama, E.-L.; Laitinen, M.; Sajavaara, T.; Karppinen, M. Control of Oxygen Nonstoichiometry and Magnetic Property of $MnCo_2O_4$ Thin Films Grown by Atomic Layer Deposition, Chem. Mater. **2010**, 22, 6297-6300.
13. Foerster, M.; Rebled, J.M.; Estradé, S.; Sánchez, F.; Peiró, F.; Fontcuberta, J. Distinct Magnetism in Ultrathin Epitaxial $NiFe_2O_4$ Films on $MgAl_2O_4$ and $SrTiO_3$ Single Crystalline Substrates, Phys. Rev. B **2011**, 84(14), 144422.
14. Rigato, F.; Estradé, S.; Arbiol, J.; Peiró, F.; Lüders, U.; Martí, X.; Sánchez, F.; Fontcuberta, J. Strain-induced stabilization of new magnetic spinel structures in epitaxial oxide heterostructures, Materials Science and Engineering: B **2007**, 144(1-3), 43-48.

15. Praus, R. B.; Leibold, B.; Gross, G. M.; Habermeier, H.U. Thickness dependent properties of $La_{0.67}Ca_{0.33}MnO_3$ thin films, Appl. Surf. Sci. **1999**, 138-139, 40-43.
16. Matvejeff, M.; Lippmaa, M.; Growth of $InFeCoO_4$ thin films on $SrTiO_3$ and MgO substrates, J. Cryst. Growth **2010**, 312(16-17), 2386-2392.
17. Wang, Y.; Li, D.F.; Dai, J.Y. Microstructure and magnetic properties of a novel spinel $(Zn,Co)Fe_2O_4$ thin film on the $SrTiO_3$ substrate, J. Cryst. Growth **2010**, 313(1), 26-29.
18. Moussy, J.B.; Gota, S.; Bataille, A.; Guittet, M.J.; Gautier-Soyer, M.; Delille, F.; Dieny, B.; Ott, F.; Doan, T.; Warin, P.; Bayle-Guillemaud, P.; Gatel, C; Snoeck, E. Thickness dependence of anomalous magnetic behavior in epitaxial Fe_3O_4(111) thin films: Effect of density of antiphase boundaries, Phys. Rev. B **2004**, 70(17).
19. Mi, S.B.; Zhang, R.Y.; Lu, L.; Liu, M.; Wang, H.; Jia, C.L. Atomic-scale structure and formation of antiphase boundaries in α-$Li_{0.5}Fe_{2.5}O_4$ thin films on $MgAl_2O_4$(001) substrates, Acta Mater. **2017**, 127, 178-184.
20. Gao, C.; Jiang, Y.; Yao, T; Tao, A.; Yan, X.; Li, X. et al., Atomic Origin of Magnetic Coupling of Antiphase Boundaries in Magnetite Thin Films, J Mater Sci Technol. **2022**, 107, 92-99.
21. Lüders, U; Bibes, M.; Bobo, J.-F.; Cantoni, M; Bertacco R.; Fontcuberta, J. Enhanced Magnetic Moment and Conductive Behavior in $NiFe_2O_4$ Spinel Ultrathin Film, Phys. Rev. B **2005**, 71(13), 134419.
22. Gatel, C.; Warot-Fonrose, B.; Matzen, S.; Moussy, J.B. Magnetism of $CoFe_2O_4$ Ultrathin Films on $MgAl_2O_4$ Driven by Epitaxial Strain, Appl. Phys. Lett. **2013**, 103(9), 092405.
23. Hoppe, M; Döring, S; Gorgoi, M.; Cramm, S.; Müller, M. Enhanced Ferrimagnetism in Auxetic $NiFe_2O_4$ in the Crossover to the Ultrathin-Film Limit, Phys. Rev. B **2015**, 91(5), 054418.
24. Rezlescu, N.; Doroftei, C.; Rezlescu, E.; Popa, P.D. Lithium ferrite for gas sensing applications, Sensors Actuat. B-Chem. **2008**, 133(2), 420-425.
25. Yousaf, M.; Naseer, U.; Li, Y. J.; Ali, Z.; Mahmood, N.; Wang, L.; Gao, P.; Guo, S. J. A Mechanistic Study of Electrode Materials for Rechargeable Batteries Beyond Lithium Ions by in Situ Transmission Electron Microscopy, Energy Environ. Sci. 2021,14, 2670-2707.
26. Teixeira, S.S.; Graça, M.P.F.; Lucas, J.; Valente, M.A.; Soares, P.I.P.; Lança, M.C.; Vieira, T.; Silva, J.C.; Borges, J.P.; Jinga, L.-I.; et al. Nanostructured $LiFe_5O_8$ by a Biogenic Method for Applications from Electronics to Medicine. Nanomaterials 2021, 11, 193.
27. Howard, S.A.; Yau, J.K.; Anderson, H.U. Structural Characteristics of $Sr_{1-x}La_xTi_{3+\delta}$ as a Function of Oxygen Partial Pressure at 1400 °C, J. Appl. Phys. **1989**, 65(4), 1492-1498.
28. Jain, S. C.; Harker, A. H.& Cowley, R. A. Misfit Strain and Misfit Dislocations in Lattice Mismatched Epitaxial Layers and Other Systems, Philosophical Magazine A, 1997, 75:6, 1461-1515.
29. Regmi, S.; Li, Z.; Srivastava, A.; Mahat, R.; Shambhu, KC.; Rastogi, A.; Galazka, Z.; Datta, R.; Mewes, T.; Gupta, A. Structural and magnetic properties of $NiFe_2O_4$ thin films grown on isostructural lattice-matched substrates. Appl. Phys. Lett. **2021**, 118, 152402.
30. Zhang, J.; Liu, W.; Zhang, M.; Zhang, X.; Niu, W.; Gao, M.; Wang, X.; Du, J.; Zhang, R.; Xu, Y. Oxygen pressure-tuned epitaxy and magnetic properties of magnetite thin films. J. Magn. Magn. Mater. **2017**, 432, 472-476.
31. Liu, K.; Zhang, R.Y.; Lu, L.; Mi, S.B.; Liu, M.; Wang, H.; Wu, S.Q.; Jia, C.L. Atomic-Scale Investigation of Spinel $LiFe_5O_8$ Thin Films on $SrTiO_3$ (001) Substrates, J Mater Sci Technol. **2020**, 40(1), 31-38.
32. Fritsch, D.; Ederer, C. Epitaxial Strain Effects in the Spinel Ferrites $CoFe_2O_4$ and $NiFe_2O_4$ From First Principles, Phys. Rev. B **2010**, 82(10), 104117.